Compared Influence of a Lubricant on Mode I and Mode II Fatigue Crack Growth Kinetics in a Gear Steel

Véronique Doquet, Maël Zaid, Vincent Bonnand, Didier Pacou, Vincent Chiaruttini, Pierre Depouhon

Author version of a paper to appear in Fatigue & Fracture of Engineering Materials & Structures.
For citation, please indicate : https://doi.org/10.1111/ffe.14541

Compared Influence of a Lubricant on Mode I and Mode II Fatigue Crack Growth Kinetics in a Gear Steel

Véronique Doquet[1], Maël Zaid[1,2,3], Vincent Bonnand[2], Didier Pacou[2], Vincent Chiaruttini[2], Pierre Depouhon[3]

[1]*Laboratoire de Mécanique des Solides, CNRS, UMR 7649, Ecole Polytechnique, Institut Polytechnique de Paris, France*

[2]*Université Paris-Saclay, ONERA, Matériaux et Structures, 92322, Châtillon, France*

[3]*Airbus Helicopters, Aéroport International Marseille Provence, 13700 Marignane*

Corresponding author: veronique.doquet@polytechnique.edu

Abstract: The influence of a helicopter gearbox lubricant on mode I or mode II fatigue crack growth in 16NCD13 steel was characterized through tests performed on SENT samples loaded in tension-compression and on cruciform samples submitted to reversed shear plus static biaxial compression, respectively. In mode I, the lubricant reduced the growth rate at low ΔK_I, and increased the threshold ΔK, while in mode II, it accelerated crack growth at low $\Delta K_{II}^{effective}$, which was not only due to a reduction in crack face friction. The upward convective flow of lubricant carrying debris exuding from the crack, a modification in oil aspect and properties, and chemical analyses near the crack front suggest that a temperature-induced degradation of the lubricant leads to a corrosive attack of the metal, which accelerates crack growth. A Tribologically Transformed Structure is observed along the lips of cracks grown in mode II with normal compression in oil.

Keywords: Mode I, mode II, fatigue crack, lubricant, corrosion, tribologically transformed structure

1. Introduction

Most of the structural pieces subjected to rolling contact fatigue are lubricated to reduce contact friction, and thus moderate surface wear. As a consequence, two families of experimental studies can be found in the literature on the influence of a lubricant and more specifically, of its viscosity and the additives it contains. Those based directly on tribological test benches reproduce rather well in service conditions, but the 3D crack path due to a complex mixed-mode loading, and its kinetics cannot be controlled *a priori*, and are rather observed *post-mortem*, and analyzed qualitatively[1-8]. By contrast, the studies based on fatigue crack growth tests on classical fracture mechanics specimens are less representative (mainly because they were generally run in pure mode I, on « 2D » cracks, in which oil pressurization is difficult to achieve), but they allow an easier comparison of crack growth kinetics in air, or in a lubricant, and an easier analysis of the observed differences, based on measured crack closure effects, and/or fractographic observations[9-13]. In addition to these experimental works, many numerical studies investigated the potential mechanical consequences of oil flow into a surface-initiated crack growing in mixed-mode towards the depth of a piece[14-23]: 1) crack growth acceleration, due either to a pressurization-induced mode I loading, if oil is forced towards the crack tip by a load rolling over the crack mouth, or 2) due to an increase of the shear-mode driving force by an oil-induced reduction of crack face friction (generally modelled simply by a reduced Coulomb friction coefficient).

More specifically in steels, lubricants were reported to reduce or increase the mode I fatigue crack growth rate to different degrees compared to ambient air, depending on 1) their composition (water or oxygen contents, additives), 2) their viscosity, which controls their penetration into the crack and the importance of their hydrodynamic wedging effect 3) the loading frequency (or the product of viscosity times the frequency[9-10], 4) the loading range (different effects in the near-threshold and Paris regimes[12-13]), and 5) the R ratio (more significant effects at low R ratio[12-13]). The observed effects were attributed either 1) to a protection of the fresh metal surfaces formed at the crack tip from oxygen or from hydrogen-releasing reactions with moist air[11], 2) to a minimization of oxide-induced closure[12-13], or 3) to a hydrodynamic crack wedging action, that would reduce the effective amplitude by truncating the bottom part of the loading cycle[9-10,12-13].

Furthermore, in structures subjected to rolling contact fatigue, cracks typically experience mixed-mode loading, with shear modes predominating due to intense hydrostatic pressure. However, despite the prevalence of such loading conditions, there appears to be a notable dearth of prior experimental studies examining the effects of lubricants on the growth kinetics of

individual cracks loaded in mode II in steels. The present study, which continues, through tests performed in a lubricant, a previous experimental and numerical work on mode II fatigue crack growth in 16NCD13 steel in air[24], seeks to address this particular research gap.

2. Experimental procedures

The tests were carried out on 16NCD13 bearing steel. The nominal chemical composition of which is indicated in Table 1. The average size of the lamellae colonies -sharing the same crystallographic orientation- in the texture-free bainitic/martensitic microstructure is 65 ± 23 μm. A conventional yield stress of 1004 MPa was measured.

TABLE 1 Nominal composition of 16NCD13 steel (weight %)

C	Si	Mn	S	P	Cr	Ni	Mo	Fe
0.16	0.28	0.48	< 0.01	< 0.02	0.96	3.14	0.23	Balance

Three millimeter-thick, 30 mm-wide Single Edge Notched Tensile (SENT) specimens (Figure 1a) were used for the assessment of the mode I fatigue crack growth threshold and kinetics in air at R = -1, using a direct current potential drop (DCPD) crack monitoring technique (Figure 1b). Such tests were also run in the lubricant used for helicopters power transmission systems: Total Aerogear 823 mineral oil with sulfur-based extreme pressure (EP) additives for gear lubrication up to moderate temperature (100 °C), whose kinematic viscosity is 63.3 mm^2/s at 40 °C, and 8.36 mm^2/s at 100 °C. The mode I fatigue crack growth tests in oil reported in the literature were conducted either by circulating the liquid and drip feeding the crack tip area[9-11], or by fully immersing the sample in an oil bath clamped to the loading train[9,11-12]. In several studies a sealed environmental chamber was used, because the oil was dehumidified *in situ* by bubbling dry helium[12], or deaerated using a vacuum pump and an argon flux[9]. The oil temperature was sometimes set at 35 °C [9] or 49 °C[11].

In the present study, since the Aerogear 823 lubricant was used as it is in service, without controlling its temperature, a much simpler device was used for the crack growth tests run in mode I (Figure 1c) as well as in mode II (Figure 2g): a small reservoir, made of two glass pieces bonded to both sides of the specimen using a silicone gasket. An opening is left at the top to pour the oil. In addition to its low cost and ease of use, the assembly offers a number of advantages. Firstly, the appropriate electrical resistance of silicone implies that wires can be

embedded in it for crack growth monitoring by the DCPD system without affecting the measurement, and its large elastic compliance allows the silicone gasket to accommodate the sample strains without damage or debonding. Secondly, the transparency of the glass plates allows direct optical tracking of the crack, or digital image correlation. Note that the Jelt brand spray paints used to make speckles were not affected by the oil bath. Finally, since the use of curved watch glasses initially resulted in unwanted light reflections, specially cut flat glass plates were used instead.

The tests were run at 2 Hz, after precracking under a decreasing ΔK_I over approximately 8.5 mm, following the ASTM E647 standard: ΔK_I was first reduced stepwise (at most by 8 % at each step), until the threshold was reached (less than 100µm growth within 2 million cycles, i.e. less than 5 10^{-11} m/cycle), then the loading range was kept constant, giving rise to an acceleration, and finally, to fracture. The stress intensity factor was not taken from a handbook, but derived from finite element simulations, in order to take the actual specimen geometry and its clamping conditions into account.

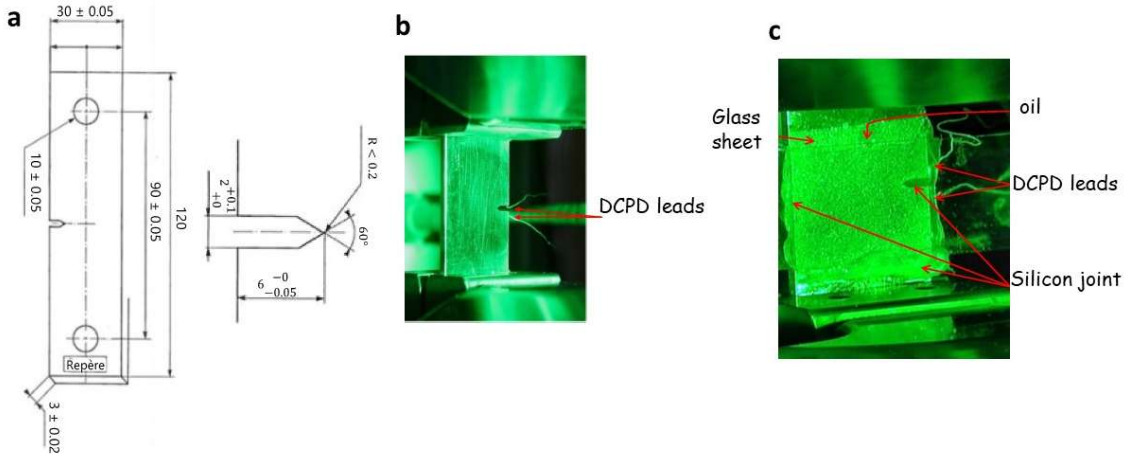

FIGURE 1 a) SENT specimen geometry used for mode I crack growth tests, b) experimental setup in air, c) detail of the experimental setup in oil

Cruciform specimens (Figure 2a) were used to investigate fatigue crack growth under reversed mode II with superimposed static biaxial-compression, to mimic the loading conditions encountered in helicopter gearboxes. Their central area (60 mm in diameter, 1.5 mm in thickness) had, in its center, a 3 mm long notch with a root radius of 100 µm, inclined by 45 °

relative to the tension/compression loading directions. One side was polished to allow direct crack growth monitoring with a spatial resolution of 16 µm/pixel, based on optical contrast, enhanced by four low-angled LED lighting sources to produce dark-field illumination. The opposite side was covered with a speckle painting to provide the necessary contrast for Digital Image Correlation (DIC) with a spatial resolution of 35.5 µm/pixel (Figure 2c). For the tests with Aerogear 823 lubricant, a small reservoir made of two watch glasses fixed on each face of the specimen by a silicon joint (Figure 2e) was nearly filled with oil before starting the test. Again, it prevented neither the capture of images for DIC, nor the direct optical monitoring of crack growth. This oil was collected and analyzed after one of the tests.

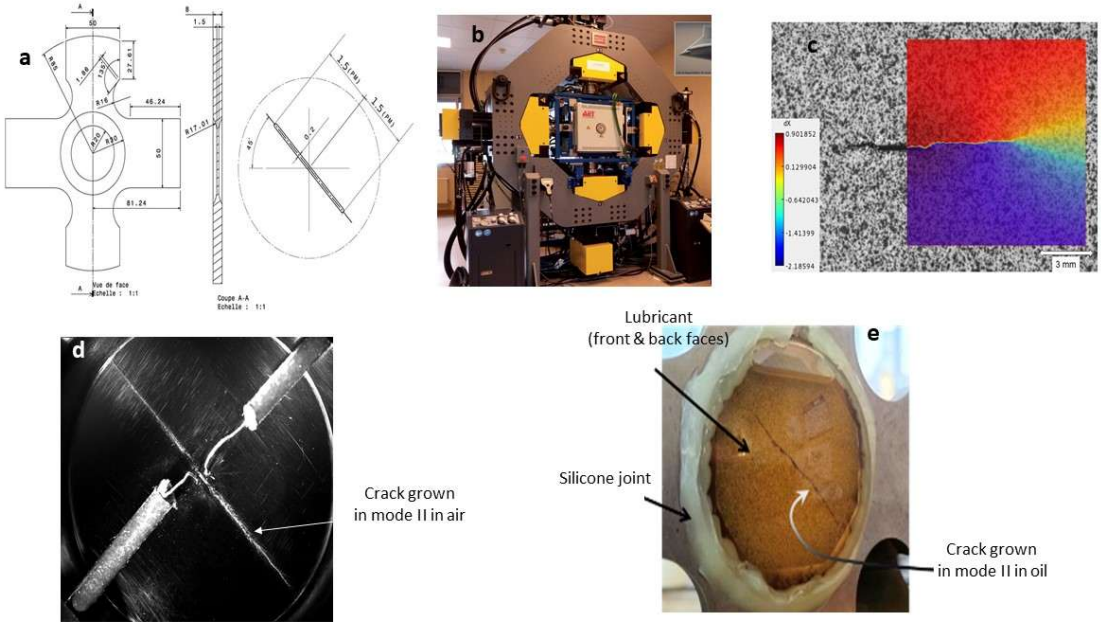

FIGURE 2 a) Cruciform specimen geometry, b) biaxial testing machine, c) sliding displacement field measured by DIC, and d-e) examples of straight, mode II crack growth obtained: d) in air (test #4 from [24]), and e) in oil (test #1, in the present paper)

The specimens were mounted on a biaxial tension-compression machine with four ±250 kN actuators (Figure 2b). Mode I precracking was first performed at $\Delta\sigma_n = 400$ MPa and $R = 0.05$, until a few millimeters long cracks had grown from both notch roots. Then, a suitable combination of loads were applied by each of the four actuators, to submit the crack to fully reversed cyclic mode II, at a frequency of 2 Hz, with either a constant (and high) shear stress amplitude (test #1, meant to investigate the upper Paris regime in oil, da/dN between 10^{-6} and

10^{-5}m/cycle), or several sequences with a regularly decreasing shear stress amplitude, following a tapered sinus wave (test #2, to investigate the lower Paris regime, in oil, down to 2.5 10^{-7} m/cycle), plus a superimposed equibiaxial static compression, as detailed in Table 2, for the two tests run in oil. The conditions of the tests previously run with the same material and protocol to establish a friction-corrected mode II crack growth kinetics in air, were detailed in Zaid et al.[24] and these will not be repeated here. Only their results (aspect of the fracture surfaces, evolutions of the apparent friction coefficient, and crack growth kinetics in air) will be used here for a comparison with the outcome of the tests run in oil.

TABLE 2 Loading conditions for the crack growth tests in oil

	Loading Sequence	$\Delta\tau$ (MPa)	Static stress along x & y (MPa)	Number of cycles	Initial crack length (mm)	Final crack length (mm)
Test #1	S 1	800	-200	3 970	4,7	18.5
Test #2	S 1	800 ↘ 512	-200	2 000	3.14	4.11
	S 2	656 ↘ 490	-200	1 400	4.11	4.83
	S 3	656 ↘ 524	-200	2 000	4.83	5.33
	S 4	800 ↘ 744	-200	1 400	5.33	10.55
	S 5	800 ↘ 736	-200	1 560	10.55	18.15

The relatively high shear stress ranges applied, favorable to mode II crack growth [25-26], but also the superimposition of a static equibiaxial compression, which hinders mode I crack growth, allowed the cracks to grow straight ahead of the notch and precrack, in mode II without bifurcation, other several millimeters, as indicated in Table 2, and illustrated by Figure 2d-e.

To determine the effective stress intensity factor $\Delta K_{II,eff}$, taking into account the crack face friction -already significant in pure mode II, due to the mere presence of asperities along the crack face, and strongly enhanced by normal compression, in the present study- image pairs were captured at minimum and maximum shear stresses, every other 10 cycles. The profiles of the relative sliding displacement amplitude of the crack face (measured using two rows of "virtual extensometers", that is: a pair of 1.2 to 2 mm-long lines, parallel to the crack, and located 0.6 mm on either side) were then obtained, as illustrated in Figure 3a.

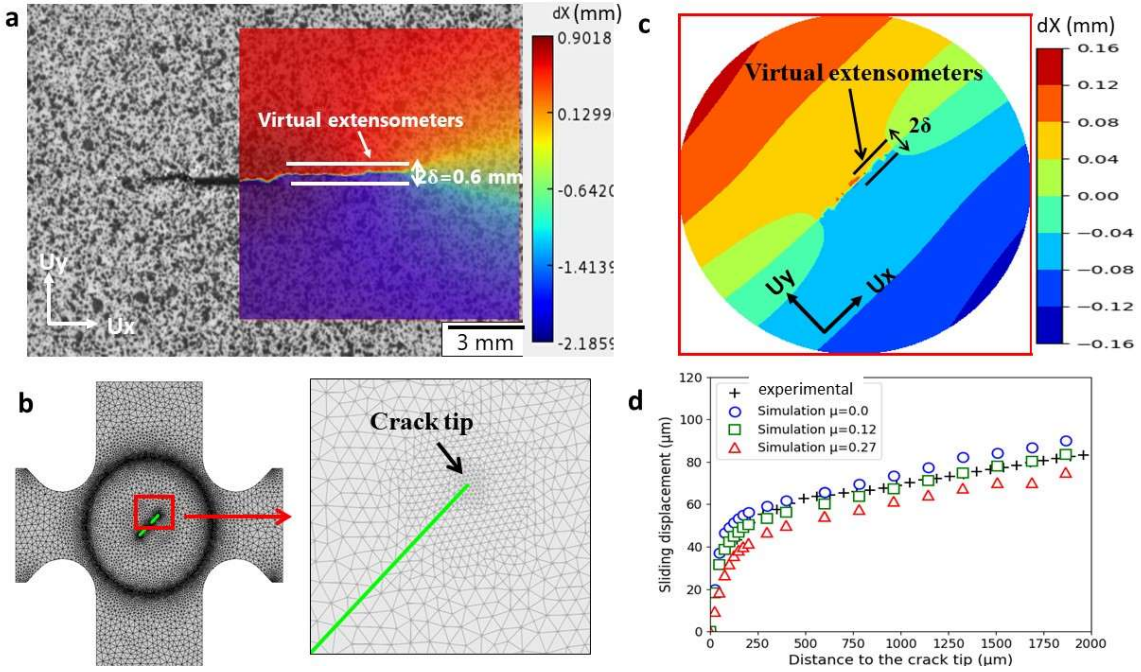

FIGURE 3 Principle of the inverse method used to determine $\Delta K_{II}^{effective}$. a) Measurement of the near-tip sliding displacement range profile, b) FE mesh of the cracked specimen, c) computation of the displacement profile by elastic-plastic simulations with various crack face friction coefficients, d) comparison with the measured profile to find the adequate value.

On the one hand, the crack face friction tends to make the real relative crack face sliding displacement range smaller than predicted by LEFM, based on $\Delta K_{II}^{nominal}$ (the value computed for a smooth, frictionless crack). On the other hand, the cyclic plasticity at the crack tip tends to make it higher than predicted by LEFM. To take into account these opposite effects and determine $\Delta K_{II}^{effective}$, 3D elastic plastic simulations of a loading cycle on the cracked cruciform specimen (meshed with linear tetrahedral elements, which are refined along the crack faces, down to 37.5 μm near the tip, Figure 3b) are first run, taking into account the actual crack length and loading range, and assuming Coulomb's friction with a uniform coefficient, μ, along the crack face. The profile of crack face relative sliding displacement amplitude is then computed as the amplitude of the sliding displacement jump between the same two rows of virtual extensometers as those used in the experiments (Figure 3c), and the computed profile is then compared to the one measured by DIC. For a given crack length, these simulations are repeated

with various values of μ (Figure 3d, where the green points correspond to a frictionless crack, which overestimates the sliding displacement, while the blue points corresponding to μ=0.27, underestimate it), until the optimum value, denoted by $\mu_{apparent,}$ is found, for which the experimental profile is best recovered (in-between 0 and 0.27 for the illustrated case). The name "apparent" is chosen to remind that this value neglects any gradient in the crack face friction. Finally, once $\mu_{apparent}$ has been determined, an elastic simulation is run with this value, and $\Delta K_{II}^{effective}$ is derived, using the G-Theta method[27], improved to take into account the fact that the crack face is not stress-free, as detailed by Vattré & Chiaruttini[28]. More details on this inverse method can be found in Bonniot et al.[29]. Finally, the measured crack growth rates can be plotted versus $\Delta K_{II}^{effective}$, allowing a comparison of friction-corrected, intrinsic mode II crack growth kinetics in air or in oil.

After the tests in mode II, observations of the crack paths on the outer surfaces, as well of the fracture surfaces were made, either with a Keyence digital optical microscope or with a FEI Quanta 600 FEG Environmental Scanning electron microscope.

3. Results and discussion

3.1.Influence of lubricant on the growth of fatigue cracks in mode I

The mode I crack growth kinetics measured in air and in oil for R = -1 are compared on Figure 4 (on which ΔK_I has been normalized by $\Delta K_{I,threshold}$, for confidentiality reasons). The presence of the lubricant appears to slow down mode I crack growth, and to increase $\Delta K_{I,threshold}$ by 40 %. The prefactor of the Paris law is reduced by a factor of 3.5 in the lubricant, while the exponent is hardly increased (from 3.01 to 3.25). Additional tests would be useful to consolidate these conclusions based on a limited set of data.

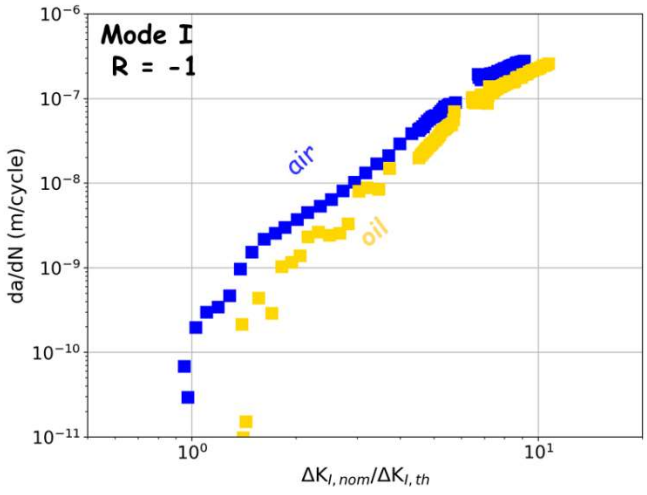

FIGURE 4 Comparison of mode I crack growth kinetics in air or in oil

SEM images of the fracture surfaces in air and oil, near the mid-thickness of the samples, for nearly the same ΔK_I are compared in Figure 5. While friction marks are clearly visible on the sample broken in air, such marks are absent from the specimen tested in oil, which suggests an efficient hydrodynamics lubrication regime, with an oil film thick enough to prevent any contact between crack faces asperities.

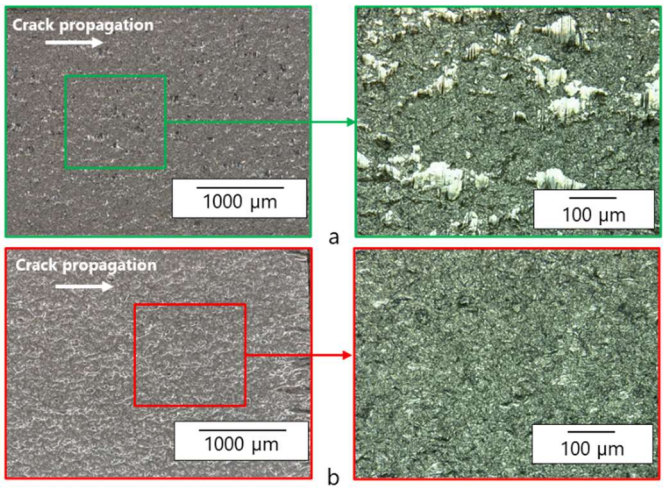

FIGURE 5 SEM observations of areas of the mode I fracture surfaces corresponding to ΔK_I = 25 MPa$\sqrt{m}$, R = -1, ad mid-thickness a) in air, and b) in Aerogear 823 oil.

Since the crack opening displacement was not monitored during this test, it is not possible to attribute with certainty the observed reduction in mode I crack growth rate in oil either to a reduction of the effective ΔK_I by the oil wedging the crack open[9-10,12-13], or to a protection of the fresh metal surfaces formed at the crack tip from detrimental reactions with moist air[11].

3.2.Influence of the lubricant on mode II fatigue crack growth.

The results of two tests run under a constant shear stress range (±500MPa, in air, ± 400MPa, in oil) plus a constant equibiaxial static compression (-200 MPa for both environments) are compared on Figure 6. In air, (Figure 6a) the apparent friction coefficient issued from the inverse analysis of measured sliding displacement profiles started from a low value (around 0.1) typical of abrasive wear, but rose steadily (up to 0.55) as the crack grew, so that the difference between $\Delta K_{II}^{nominal}$ and $\Delta K_{II}^{effective}$ (denoted as $\Delta K_{II}^{friction}$) increased, even though

$\Delta K_{II}^{nominal}$ rose. This was attributed[24] to the fact that crack lip oxidation is less and less pronounced, as the crack grows (as illustrated by the difference in grey level between the two zoomed images extracted from the SEM-BSE image provided in Figure 6a). Again, friction between two bare metal surfaces is known to be more intense, due to adhesive forces, than when an oxidized third body layer is present in-between.

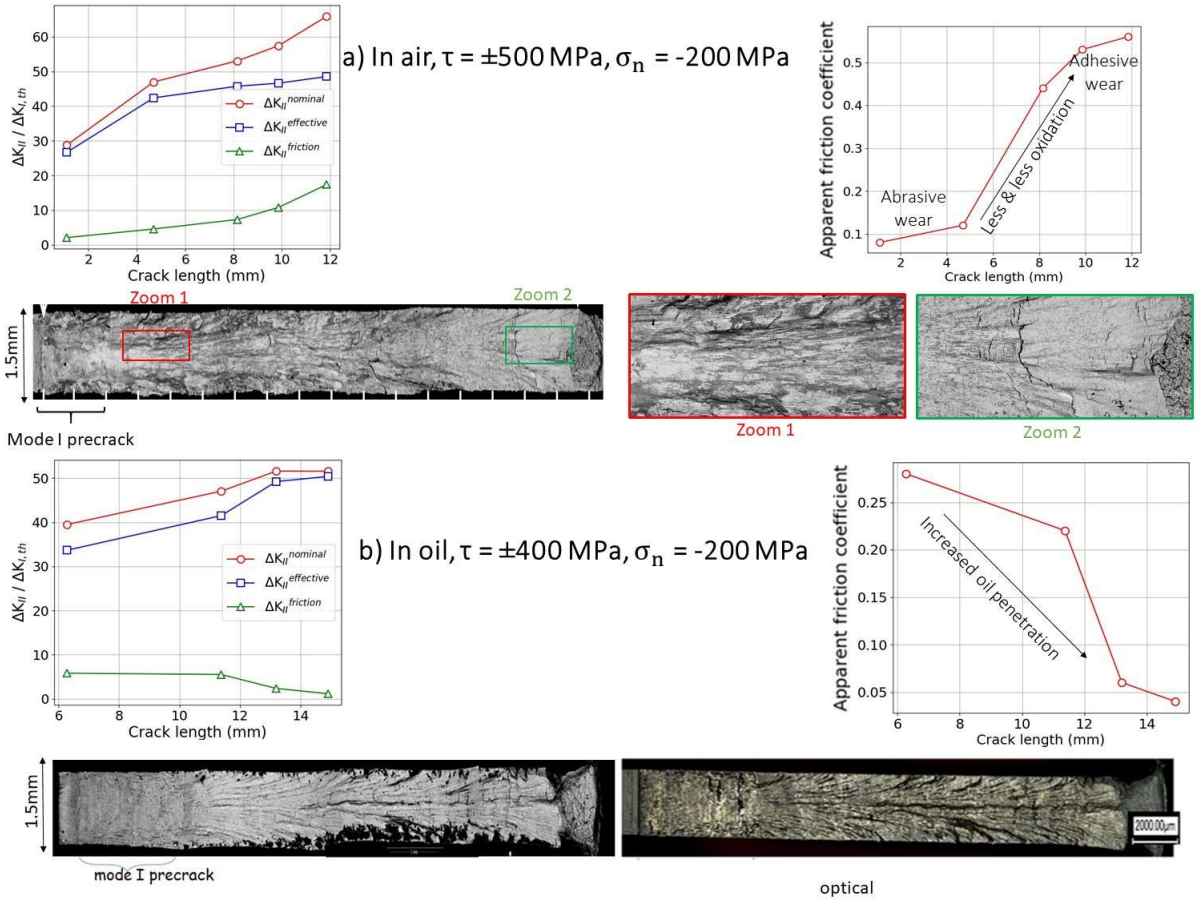

FIGURE 6 Compared results of two crack growth tests in mode II, under a constant shear stress range and constant equibiaxial static compression in air, a) and in oil (test #1), b)

By contrast, after the test run in oil (Figure 6b, in which both a SEM-BSE image captured just after the specimen was opened, and an optical microscopy image captured after cleaning are shown), no adherent oxide layer seemed to be present, but rather dark-looking debris accumulated near both side surfaces. The fracture surface looked much less mated than in air. Similar observations were made by Smith and Smith[30] who performed crack growth tests in repeated mode II ($R \approx 0$) with in-phase normal compression on pure aluminum in air, or in mineral oil.

Here, the fracture surface exhibits more or less symmetrical, up to several millimeters long wear marks curved towards the side surfaces, above and below the mid-thickness line. The direction of these marks reflects the local sliding displacement direction, controlled by the local mode mixity ratio K_{II}/K_{III}. Indeed, as illustrated by Figure 7, like for any specimen containing a through crack loaded in mode II, a 3D coupling effect controlled by the Poisson's ratio, and independent of the crack length induces a skew-symmetric distribution of K_{III}, which increases from the sample mid-thickness -where pure mode II prevails, and where the wear marks are parallel to the free surfaces -towards the free surfaces, where the wear marks are inclined, and the energy release rate approximately 12 % higher than at mid-thickness.

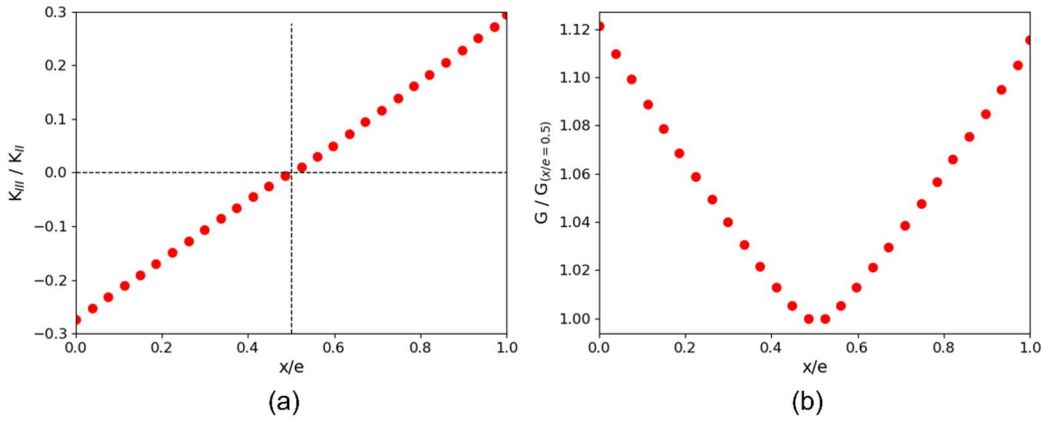

FIGURE 7 Computed profiles of a) K_{III}/K_{II} and b) the normalized energy release rate G, along the crack front, assumed here to be straight, in the cruciform specimen, for any crack length.

As discussed in the following, the oil film does not seem to be thick enough to prevent any contact between asperities along the entire crack length and thus suppress the formation of wear debris, as in the study by Smith and Smith[30]. The long-range ratchetting, to and fro dragging of the debris on the fracture surfaces by the cyclic sliding displacements is probably responsible for the formation of such long, skew symmetric, curved wear marks. However, the lubricant seems to prevent their adhesion to the metal surface and favor their ejection by transporting it towards both side surfaces.

During test #1, $\mu_{apparent}$ had a moderate value (around 0.3) at the first analyzed step (about 6mm crack length), and then kept decreasing to finally vanish as the crack grew. The observation of continuous upward convective transport by oil of dark debris emerging from the crack faces, illustrated by Figure 8a (and more visible on a video presented as supplementary material)

suggested an explanation. Convective upward transport means that a sharp thermal gradient exists in the immediate vicinity of the crack, which suggests a significant friction-induced heating of the metal surfaces, and thus, locally, of the lubricant. Since the kinematic viscosity of the lubricant decreases sharply as the temperature rises (by a factor of 7.5 between 40 and 100 °C), this makes the oil flow into the crack easier and easier, so that the fraction of the crack length, $r = \frac{infiltrated\ len}{crack\ length}$, which is infiltrated -and thus, more or less lubricated, to a degree discussed below-, should rise, leading to the observed drop of $\mu_{apparent}$. The length of the crack into which oil penetrates was estimated from the video images, as the length of the crack made visible by the exudence of oil loaded with dark debris (oil behaves more or less similar to a dye penetrant). Then, the "infiltrated fraction", r, was deduced. Its increase for test #1 correlates well with the decrease of $\mu_{apparent}$, as shown by Figure 8b.

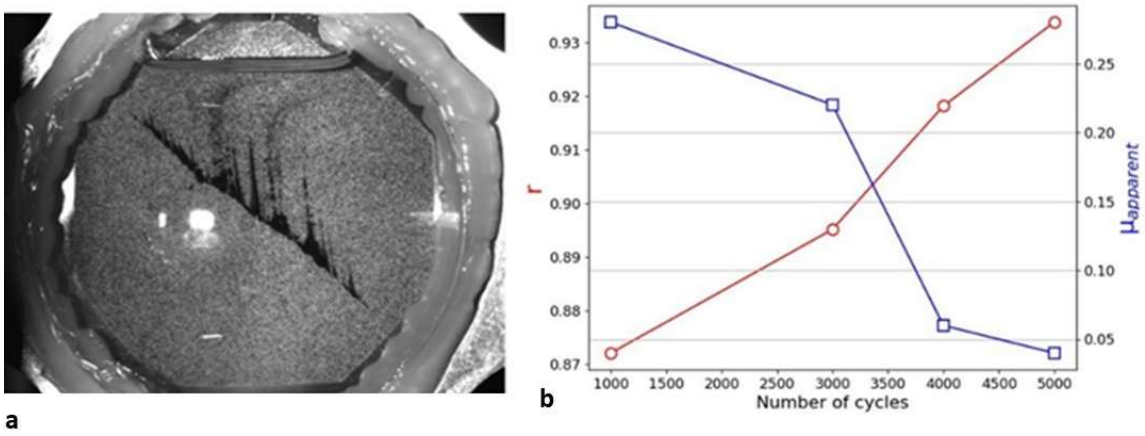

FIGURE 8 a) convective upward transport by oil of debris emerging from a crack growing in mode II with static biaxial compression (test #1), and b) compared evolutions of $\mu_{apparent}$ and of the infiltrated fraction of the crack length.

The video presented as supplementary material also shows that the upward convective transport of debris by oil initiates from discrete and steady points along the crack face, with new debris emergence sites appearing as the crack grows. These discrete "source points" might either correspond to the areas where the curved wear marks mentioned above (Figure 6b), which might constitute "debris transport channels" meet the side surfaces, or as the position of contacting crack face asperities, where the "flash temperatures" are reached. The persistent activity of many "source points" as they are left behind by the propagating crack front, agrees

better with the first interpretation, since asperities would be expected to fracture or wear, and thus stop inducing high temperatures.

During test #2, due to an imperfect load control during the precracking stage, the precrack was not perfectly aligned with the notch, but inclined by approximately 12 degrees. During sequence #1, in mode II + biaxial compression, the crack progressively recovered an orientation parallel to the notch, giving rise to a complex 3D crack face shape (Figure 9a and b). Since the inverse analysis of sliding displacement profiles assumes a flat crack face, normal to the outer surfaces, the computed values of the apparent friction coefficient were not considered reliable for sequence 1 and probably for sequence 2 as well. Figure 9d shows that during sequences 3 and 4, the apparent friction coefficient kept decreasing until it vanished, as during test #1. At first sight, this may seem surprising, considering the seemingly increasing crack face "roughness", illustrated by two transverse sections (Figure 9c), at the positions indicated by green lines on Figure 9a, at 5 and 12 mm from the notch root, corresponding respectively to $\frac{\Delta K_{II,eff}}{\Delta K_{I,th}} = 3.1$ and $\frac{\Delta K_{II,eff}}{\Delta K_{I,th}} \approx 36.5$. However, as the crack propagates, the crack face rather exhibits more and more long-range waviness, than an increasing roughness, with sharper or more numerous asperities. But above all, since the wear-induced furrows are parallel to the local sliding displacement direction, it should not hinder sliding as a random roughness would do. Therefore, it is not incompatible with the observed decrease of $\mu_{apparent}$.

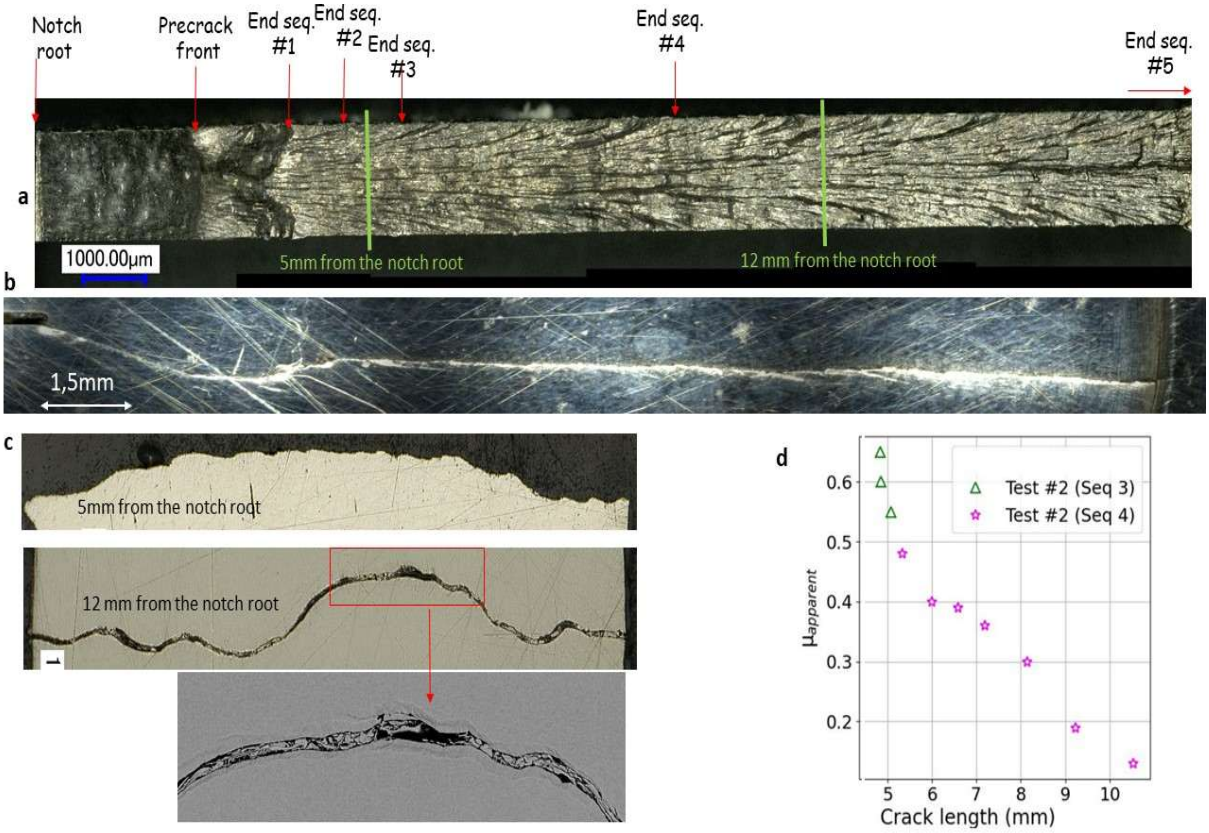

FIGURE 9 a) Fracture surface after shear mode crack propagation in oil (test #2), b) crack path observed on a side surface c) transverse sections at two stages (marked by green lines on Figure 10a**.** Note the flake-like, folded metal debris trapped between the two crack lips on the zoomed SEM image), and d) corresponding evolution of the apparent friction coefficient

Figure 10 shows the results of an Electron Back Scattering Diffraction (EBSD) analysis run with a step size of 75 nm, on a 60*20 µm area straddling both crack lips on the transverse section cut at a=12 mm. For that purpose, the sample has been embedded in resin, and prepared by mechanical and ion polishing. Grain boundaries and subgrain boundaries were defined based on 5 degrees or 2 degrees misorientation, respectively. The Grain Orientation Spread (GOS, which is the average over all pixels of a grain of their deviation from the mean orientation) was computed, and three types of grains were labelled in different colors: those with a GOS smaller than 3 ° were considered as recrystallized and plotted in blue, those containing recrystallized sub-grains misoriented by more than 3 ° relative to one another were plotted in yellow, and those with a GOS larger than 3 ° and no subgrains were considered as deformed, and plotted in red.

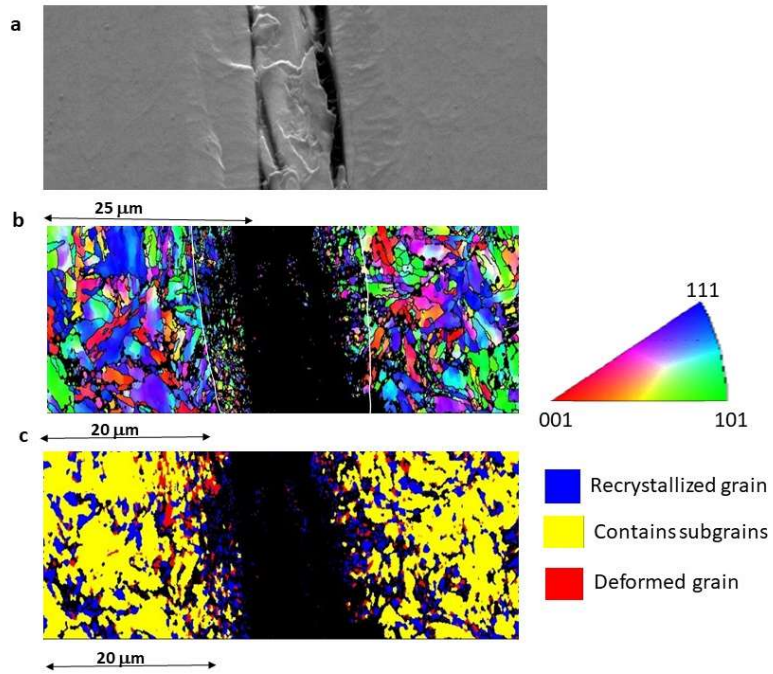

FIGURE 10 EBSD analysis of a 60*20 µm area of the transverse section at a=12 mm, captured with a step size of 75 nm, a) electron image, b) Inverse pole figure and c) grain condition: blue = recrystallized grain, yellow: contains sub-grains, and red= deformed grain.

On Figure 10b and c, we notice the presence of a 4 to 5 µm wide layer of recrystallized and strongly refined grains (less than 100 nm, making their indexation difficult with EBSD), which is due to a dynamic recrystallization, induced by contact stresses, in other words: the formation of what tribologists observe after fretting tests, and name a Tribologically Transformed Structure, or TTS[31-34]. Preliminary observations of the same type on other transverse sections suggest that the TTS becomes thicker, as the distance to the final crack front increases. Work is in progress to document and analyze this point. During fretting tests, the steady-state thickness of the TTS layer is controlled by two opposite effects: a progressive transformation of the severely sheared metal located below the TTS into TTS, and the microcracking and spalling of the TTS itself, favored by its poor ductility and toughness, which releases metal debris. The development of a TTS along the crack face in the present case is consistent with the conclusion from Shipway et al.[34] that TTS tends to develop along oxygen-deprived sliding contacts, due to the lack of oxidized third-body layer, which would protect the metal itself.

These observations show that intense contact stresses can exist along the crack growing in mode II under normal compression in a lubricant, while $\mu_{apparent}$ tends to decrease as the crack grows.

This parameter does not pretend to be more than a convenient fictitious parameter allowing to capture, in average over 1 to 1.5 mm behind the tip, the effect of friction on the near tip sliding displacement, and on the effective crack driving force.

Figure 11 shows that $\mu_{apparent}$ exhibits an inverse correlation with $\Delta K_{II}^{effective}$ or with da/dN.

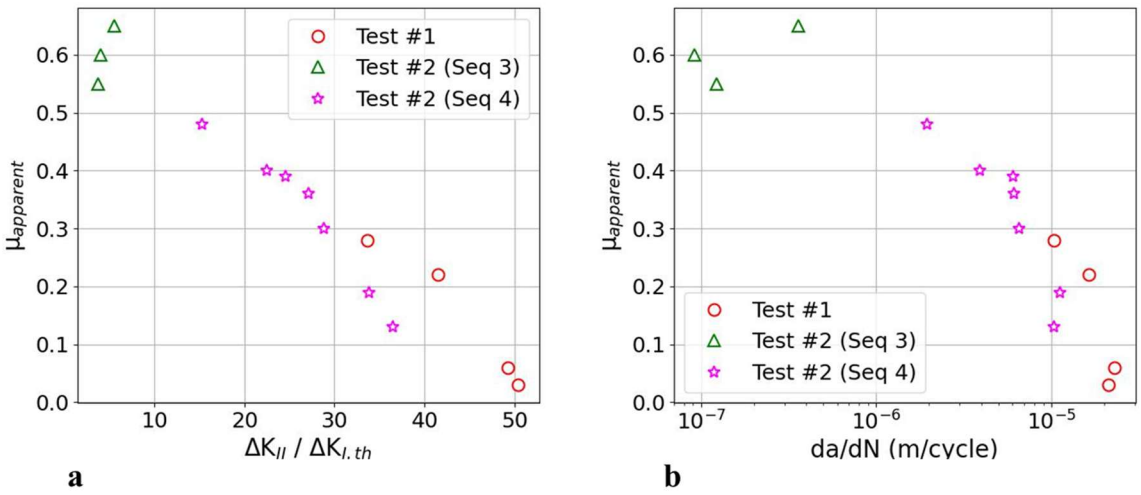

FIGURE 11 Correlation between $\mu_{apparent}$ and a) $\Delta K_{II}^{effective}$, or b) da/dN

Several tribological studies[35-37] of lubricated fretting contacts (reciprocating sliding tests in oil or grease run on bearing steels) have shown that the sliding amplitude has a major effect on the friction coefficient: in the gross slip regime, the higher the amplitude and the sliding rate, the easier and faster the penetration of the lubricant into the whole contact area, and the development of a homogeneous protective tribofilm, resulting in a reduced friction coefficient. The influence of ΔK_{II}^{eff} described by Fig. 11, as well as the increase in oil penetration reported on Fig. 8b as the crack grows (and thus as ΔK_{II}^{eff} rises) are consistent with those studies, since the sliding amplitude at any point along the crack face is directly proportional to ΔK_{II}^{eff}.

The friction-corrected mode II crack growth kinetics in air and in oil are compared in Figure 12. Since the effect of the lubricant on crack face friction has already been taken into account, by using an effective ΔK_{II}, the acceleration of mode II crack growth that it induces, when the growth rate is less than approximately 3 μm/cycle, has a different origin, which is discussed later, based on the chemical analyses reported below.

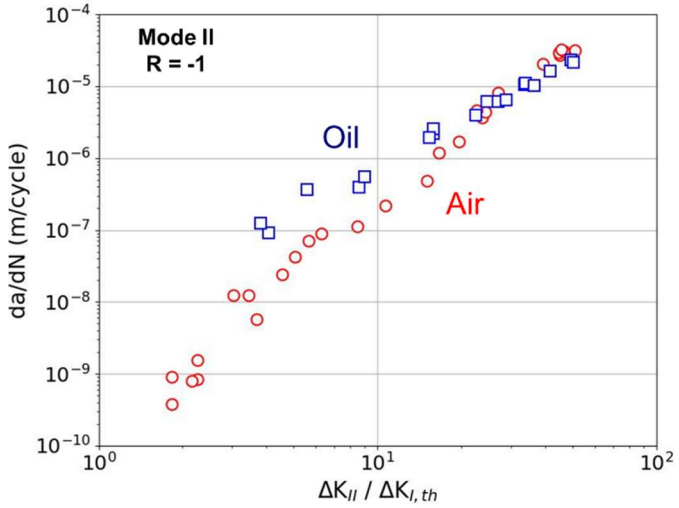

FIGURE 12 Compared friction-corrected mode II crack growth kinetics in air and in oil, at 2Hz and R= -1, for 16NCD13 steel

Two reasons could be invoked to explain the acceleration of mode II crack growth by the lubricant. Mode I loading, induced by oil trapping and pressurization should be envisaged, as in many previous papers on crack growth in rolling contact fatigue mentioned in the introduction[14-23]. However, in such studies, a surface-initiated crack growing towards the depth of a bulk structure was considered, so that the lubricant flowing from the surface into the crack could not escape, and could only be forced towards the crack front, by a heavy load rolling over the crack mouth. The situation is quite different in the present study, since the thickness of the cruciform specimens is only 1.5 mm, so that the oil should be able to flow away easily from the crack faces through the side-surfaces. Furthermore, the equibiaxial compression is permanent here, and might squeeze the oil film out of the crack, which is not the case in rolling contact fatigue of structures, in which compression is generally intermittent, making the infiltration of oil much easier. So, in the present case, even though small amounts of oil might temporarily be trapped here and there in hollows along the crack face and induce some very localized overpressure, this explanation does not seem plausible.

An alternative explanation is based on a mechanically and thermally-induced chemical degradation of the lubricant, designed to be used only up to 100°C, while the convective currents observed during the tests suggest a significant heating at a local scale. The oil used during test #2 on the back face, which had little contact with speckle painting was collected, and even though the total cycling time was only 70 minutes (8360 cycles at 2 Hz), its color was

significantly altered (Figure 13a). It became darker, partly -but not only- due to debris exuded by the crack. Figure 13b compares the absorbance spectra of fresh and used oil, collected with an infrared spectrometer. Some differences can be observed, meaning that the lubricant was indeed altered during the shear mode crack growth test, not in the wavelength range expected in case of oil oxidation though (between 1670 and 1760 cm^{-1}), but rather for absorbance peaks related to C-O and C-C bonds. The viscosities were measured with a Fludicam Rheo Viscosimeter (with at least 5 repeated measurements in each case) as: 178 ± 3.4 cP for the fresh oil, and 138.7 ± 4.4 cP for the oil collected on the paint-free back side. The lubricant viscosity was thus reduced by 22.5 % during the crack growth test, which suggests a reduction in the length of molecular chains.

Kohara[5] and Lu et al.[6-7] have shown that the alteration of C_nH_m hydrocarbon molecules from the lubricants in sliding contacts releases various gases, among which hydrogen that can diffuse into the steel and to embrittle it, because of 1) oil decomposition by a catalytic reaction with fresh metal surfaces (specially at crack fronts), 2) break of molecular chains by shear and 3) a thermal decomposition caused by the heat generated by friction. Note that except maybe for the first cause, mode I loading is far less likely than mode II to degrade a lubricant, and to release hydrogen.

Thanks to their high reactivity, which is further increased when the temperature rises, various additives in the lubricant can postpone its decomposition and a slow-down hydrogen release[5-6]. Meheux et al.[2], as well as Lhostis et al.[1] performed local chemical analyses along cracks naturally initiated from the surface of steel samples during rolling contact fatigue tests run in lubricants with sulfur-based extreme pressure additives and reported an increase in the amount of sulfur towards the crack tip. According to Meheux et al.[2], when a nascent, very reactive metal surface is created at the crack front, it reacts with sulfur, forming iron sulfides, and a protective tribofilm, whose thickness increases from a few nanometers, close to the tip, to more than 100 nm, close to the crack mouth. Lhostis et al.[1] concluded that such a film could act as a barrier to hydrogen permeation into the metal.

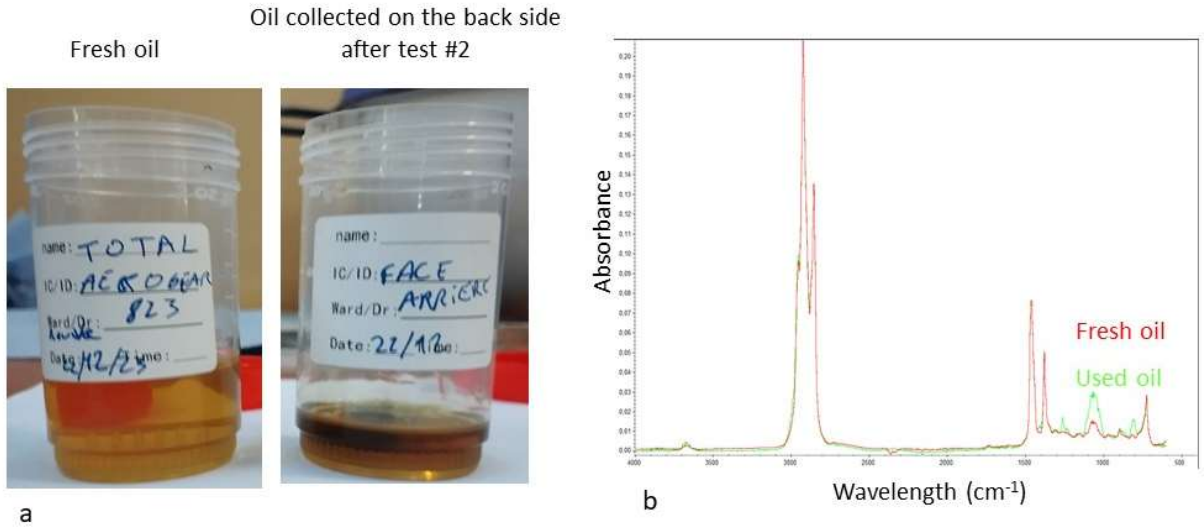

FIGURE 13 a) Compared aspects of fresh and used lubricant (collected after test #2 on the back side), and b) compared infrared absorbance spectra

In the present study, microscale chemical analyzes were performed on the two mating fracture surfaces of sample #2, using Energy Dispersive Spectroscopy (EDS) in the SEM, near the final crack front (Figure 14), on both fracture surfaces of sample #2. While no significant heterogeneity in the distribution of Fe, O, C, Cr, Si and Ni could be detected, a sulfur segregation was clearly observed on both crack faces, confirming the formation of a tribofilm.

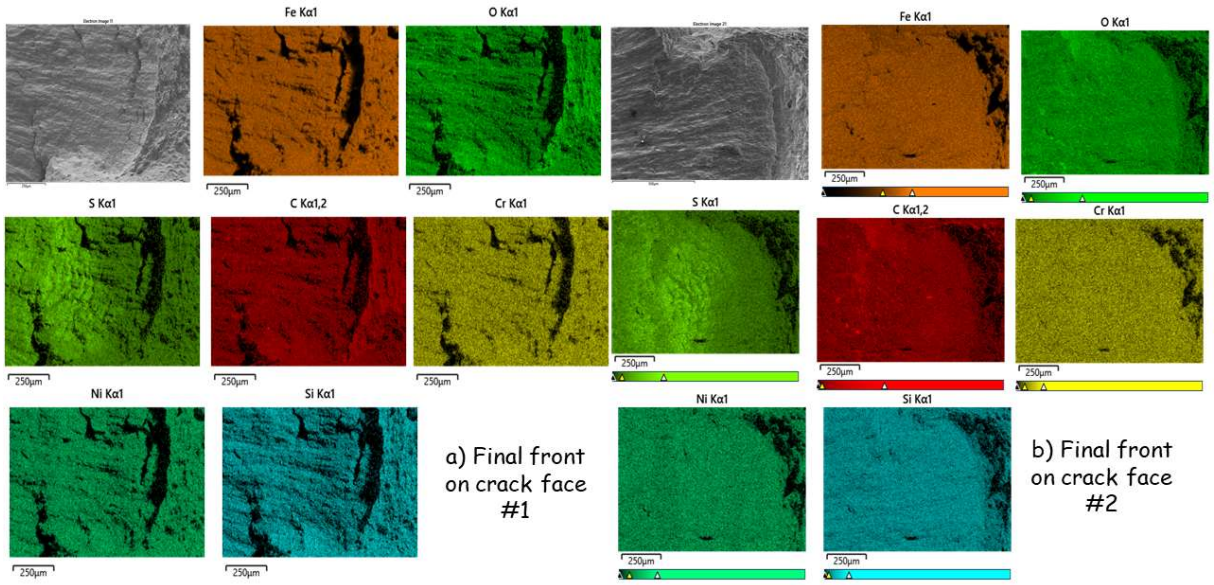

FIGURE 14 EDS mapping of the distribution of various elements near the final crack front of sample #2 on a) crack face #1, and b) crack face #2

However, the protective effect of this film against fresh-metal surface-catalyzed release of hydrogen can be questioned, considering the presence of many areas along the crack face, where the sulfur-based tribofilm seems discontinuous. As an example, Figure 15 was captured close to aluminum and titanium oxide inclusions and shows two areas with different aspects and different sulfur coverage rates: a relatively smooth area that exhibits parallel friction marks, where sulfur is clearly present and a rougher, pitted area with much less sulfur. Hard debonded oxide inclusions might scratch the surface and break the tribofilm.

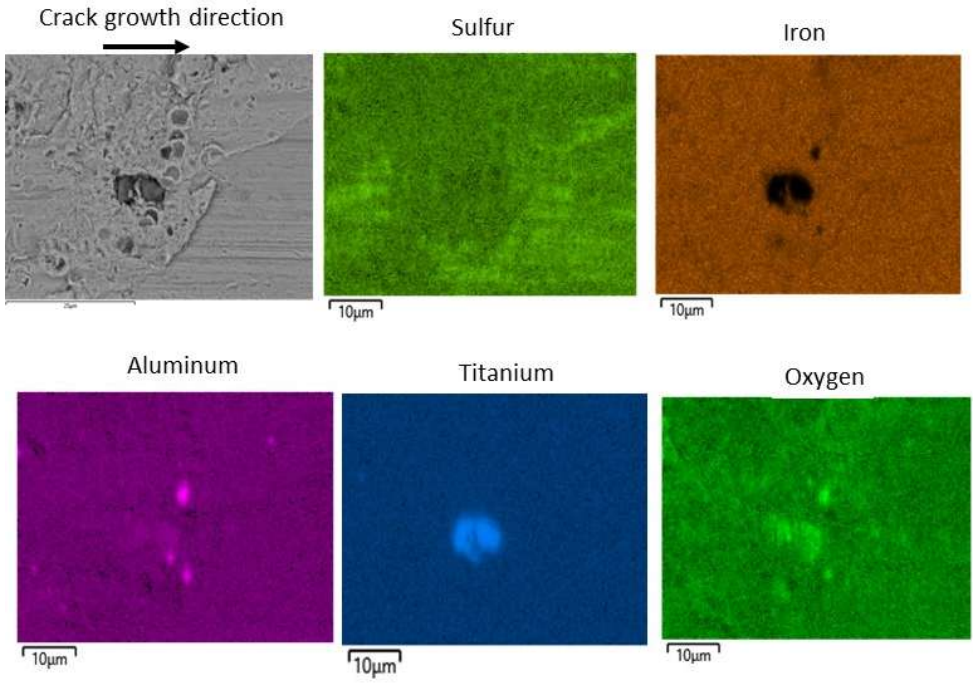

FIGURE 15 EDS mapping of the distribution of various elements in an area where the sulfur-based tribofilm seems discontinous

Tuszinski et al.[8] wrote "EP type lubricating additives are known for their high corrosion aggressiveness. It leads to the creation on the lubricated surface of numerous depressions and micro pits due to corrosive wear". Torrance et al. [4] also noted that the chemical reactivity of EP additives can be too high, and cause depressions and micro pits on the lubricated surfaces, leading to corrosion-enhanced fatigue.

4. Conclusions

Fully-reversed mode I and mode II fatigue crack growth tests run on at 2 Hz on 16NCD13 steel, in air or in a lubricant for helicopter gear boxes, analyzed by elastic-plastic FE simulations with crack face friction, and followed by fractographic observations and chemical analyses have shown that:

- The lubricant seems to reduce the mode I crack growth rate at low ΔK_I, and to increase $\Delta K_{I,threshold}$ by 40 %. These effects, which need to be confirmed by additional tests, might be due either to a reduction of the effective ΔK_I by the oil wedging the crack open, or to a protection of the fresh metal surfaces formed at the crack tip from detrimental reactions with moist air.
- On the contrary, the lubricant accelerates crack growth in mode II, when it is slower than 3.10^{-6} m/cycle. This is not only due to a reduction of crack face friction, but quite probably as well to a chemical attack by the degraded lubricant, possibly associated with hydrogen release, because of intense shearing and friction-induced heating.
- Surprisingly, for tests run in the lubricant, the contact stresses during mode II crack growth with static biaxial compression were sufficient to generate a Tribologically Transformed Structure (TTS), with ultrafine grains, along each crack face. Work is in progress to document and analyze the evolution of the thickness of this layer with the distance to the final crack front.
- While lubrication is essential to protect helicopter gearboxes against wear and contact surface damage, it could also favor subsurface crack growth, in mode II. This concern is amplified by the elevated loading frequency inherent to gearboxes bearings, which may intensify heat dissipation along the crack faces, consequently hastening the degradation of the lubricant. Since the lubricant plays a key role in the evolution of such damage, particular attention should be paid to the representativeness of environmental conditions of the tests run to determine the crack growth kinetics used for safety assessment of critical parts.

AUTHOR CONTRIBUTIONS

Véronique Doquet: Conceptualization, Formal analysis, Investigation, Methodology, Visualization , Writing – original draft. **Maël Zaid:** Conceptualization, Data curation, Formal analysis, Investigation, Methodology, Software, Visualization. Writing - review & editing. **Vincent Bonnand :** Conceptualization, Data curation, Investigation, Methodology. Writing -

review & editing. **Didier Pacou:** Investigation, Methodology. **Vincent Chiaruttini** : Conceptualization, Formal analysis, Methodology, Software, Writing – review & editing. **Pierre Depouhon** : Conceptualization, Funding acquisition, Project administration, Ressources, Writing –review & editing.

ACKNOWLEDGMENTS

This work was supported by Airbus Helicopters and by ANRT (CIFRE PhD grant N° 2019/0261 for Maël Zaid). The support of Alexandre Tanguy and Simon Hallais from the Laboratoire de Mécanique des Solides to SEM observations, as well as EDS and EBSD analyses is gratefully acknowledged.

DATA AVAILABILITY.

Industrial secrecy considerations do not allow the dissemination of data.

References

1. L'Hostis B, Minfray C, Fregonese M, Verdu C, Ter-Ovanessian B, Vacher B, Le Mogne T, Jarnias F, Da-Costa D'Ambros A. Influence of lubricant formulation on rolling contact fatigue of gears- interaction of lubricant additives with fatigue cracks. *Wear* 2017;382–383:113–122.

2. Meheux M, Minfray C, Ville F, Le Mogne T., Lubrecht AA, Martin JM, Lieurade HP, Thoquenne G, Effect of lubricant additives in rolling contact fatigue. *Proc Inst Mech Eng Part J. J. Eng. Tribol.* 2010;224:947–955.

3. Cornelio C, Spagnuolo E, Di Toro G, Nielsen S, Violay M. Mechanical behaviour of fluid-lubricated faults. *Nature Comm.* 2019;10:1274.

4. Torrance AA, Morgan JE, Wan G.T.Y. An additive's influence on the pitting and wear of ball bearing steel. *Wear* 1996;192:66–73.

5. Kohara M, Kawamura T, Egami M. Study on mechanism of hydrogen generation from lubricants. *Tribol. Trans.* 2006;49:53–60.

6. Lu R, Mori S, Kubo T, Nanao H. Effect of sulfur-containing additive on the decomposition of multialkylated cyclopentane oil on the nascent steel surface. *Wear* 2009;267:1430–1435.

7. Lu R, Nanao H, Kobayashi K, Kubo T, Mori S. Effect of lubricant additives on tribochemical decomposition of hydrocarbon oil on nascent steel surfaces. *J Jpn. Pet. Inst.* 2010;53:55–60.

8. Tuszynski W, Michalczewski R, Piekoszewski W, Szczerek M. Effect of ageing automotive gear oils on scuffing and pitting. *Tribol. Int.* 2008;41:875–888.

9. Endo K, Okada T, Komai K, Kiyota M. Fatigue crack propagation of steel in oil. *Bull. JSME* 1972; 15(89):1316-23.

10. Endo K, Okada T, Hariya T. Fatigue crack propagation in bearing metals lining on steel plates in lubricating oil. *Bull. JSME* 1972;15(82):439-445.

11. Polk CJ, Murphy WR, Rowe CN. Determining fatigue crack propagation rates in lubricating environments through the application of a Fracture Mechanics Technique. *ASLE Trans.* 1975;18(4):290-298.

12. Tzou JL, Suresh S, Ritchie RO. Fatigue crack propagation in oil environments –I. Crack growth behavior in silicone and paraffin oils. *Acta Met.* 1985;33(1):105-116.

13. Tzou JL, Hsueh CK, Evans AG, Ritchie RO. Fatigue crack propagation in oil environments –Part II. A model for crack closure induced by viscous fluids. *Acta Met.* 1985;33(1): 117-127.
14. Kaneta M, Murakami Y. Effects of oil hydraulic pressure on surface crack growth in rolling/sliding contact. *Tribol. Int.* 1987;20:210–217.
15. Bower AF. Influence of crack face friction and trapped fluid on surface initiated rolling contact fatigue cracks. *J. Tribol.* 1988;110:704-711.
16. Omidvar B, Ghorbanpoor A. The role of oil seepage in fatigue crack growth of lubricated wearing systems. *Engng. Fract. Mech.* 1998;60:239-250.

17. Ren Z, Glodez S, Fajdiga G, Ulbin M. Surface initiated crack growth simulation in moving lubricated contact. *Theoretical & Applied Fract. Mech.* 2002;38:141–149.
18. Bogdañski, S. A rolling contact fatigue crack driven by squeeze fluid film: A RCF crack driven by squeeze fluid film. *Fatigue & Fract Engng Mater. & Struct.* 2002;25:1061–1071.

19. Bogdański, S., Lewicki, P. and Szymaniak, M. Experimental and theoretical investigation of the phenomenon of filling the RCF crack with liquid. *Wear* 2005;258:1280–1287.

20. Bogdański, S. and Lewicki, P. 3D model of liquid entrapment mechanism for rolling contact fatigue cracks in rails. *Wear* 2008; 265:1356–1362.

21. Dubourg MC, Lamack V. A Predictive Rolling Contact Fatigue Crack Growth Model: Onset of Branching, Direction, and Growth—Role of Dry and Lubricated Conditions on Crack Patterns. *Trans. ASME* 2002;124: 680-688.

22. Ringsberg JW. Shear mode growth of short surface-breaking RCF cracks. *Wear* 2005;258:955–963
23. Ancellotti S, Benedetti M, Dallago M, Fontanari V. The role of the second body on the pressurization and entrapment of oil in cracks produced under lubricated rolling-sliding contact fatigue. *Theoretical & Applied Fract. Mech.* 2017;91: 3–16.

24. Zaid M, Bonnand V, Doquet V, Chiaruttini V, Pacou D, Depouhon P. Fatigue crack growth in bearing steel under cyclic mode II + static biaxial compression. *Int. J. Fatigue* 2022;163: 107074, https://doi.org/10.1016/j.ijfatigue.2022.107074

25. Pinna C, Doquet V. The preferred fatigue crack propagation mode in a M250 maraging steel loaded in shear. *Fatigue Fract. Engng. Mater. Struct.* 1999;22:173-183. https://doi.org/10.1046/j.1460-2695.1999.00161.x

26. Doquet V., Bertolino G. A material and environment-dependent criterion for the prediction of fatigue crack paths in metallic structures. *Engng. Fract. Mech.* 2008;75:3399–3412. doi:10.1016/j.engfracmech.2007.07.004.

27. Destuynder, Ph., Djaoua, M. and Lescure, S. Quelques remarques sur la mécanique de la rupture élastique. *Journ. Mécanique Théorique & Appliquée* 1983;2:113–135

28. Vattré A, Chiaruttini V. Singularity-free theory and adaptive finite element computations of arbitrarily-shaped dislocation loop dynamics in 3D heterogeneous material structures. *J. Mech. Physics Solids*, 2022;167:104954. https://doi.org/10.1016/j.jmps.2022.104954

29. Bonniot T, Doquet V, Mai SH. Determination of effective stress intensity factors under mixed-mode from digital image correlation fields in presence of contact stresses and plasticity. *Strain* 2020; 56:e12332. https://doi.org/10.1111/str.12332

30. Smith MC, Smith RA. The formation of spherical wear debris in mode II fatigue cracks. *Wear* 1982;76:105–128
31. Sauger E, Fouvry S, Ponsonnet L, Kapsa P, Martin JM, Vincent L. Tribologically transformed structure in fretting. *Wear* 2000;245:39–52
32. Xin L, Wang ZH, Li J, Lu YH, Shoji T. Fretting wear behavior and mechanism of Inconel 690 alloy related to the displacement amplitude. *Tribol. Trans.* 2017;60:913-922
33. Descartes S, Busquet M, Berthier Y. An attempt to produce ex situ TTS to understand their mechanical formation conditions – The case of an ultra-high purity iron. *Wear* 2011;271:1833–1841
34. Shipway PH, Kirk AM, Bennett CJ, Zhu T. Understanding and modelling wear rates and mechanisms in fretting via the concept of rate-determining processes – contact oxygenation, debris formation and debris ejection. *Wear* 2021;486-487:204066
35. Liu QY, Zhou ZR, Effect of displacement amplitude in oil-lubricated fretting, *Wear* 200;239:237-243
36. Haviez L, Fouvry S, Yantio G, Investigation of grease behavior under simple and complex displacement amplitudes conditions, *Tribol. Int.* 2016;100: 186-194
37. Shima M, Suetake H, McColl IR, Waterhouse RB, Takeuchi M, On the behavior of an oil lubricated fretting contact, *Wear* 1997;210: 304-310